# Meson production in proton-nucleus and nucleus-nucleus collisions



1993 Phys. Scr. 48 194

(http://iopscience.iop.org/1402-4896/48/2/014)

Physica Scripta. Vol. 48, 194–199, 1993

# Meson Production in Proton–Nucleus and Nucleus–Nucleus Collisions*

W. Cassing†

Institut für Theoretische Physik, Universität Giessen, Germany

*Received August 28, 1992; accepted November 11, 1992*

## Abstract

The production of $K^+$ or $\eta$ mesons in proton–nucleus reactions is analysed with respect to primary nucleon–nucleon ($NN \rightarrow N\Lambda K^+$ or $NN\eta$) and secondary pion–nucleon ($\pi N \rightarrow K^+\Lambda$ or $\eta N$) production channels on the basis of a phase–space model employing Hartree–Fock groundstate momentum distributions and free on-shell production processes. The phase–space model adopted here compares well for meson production with more involved simulations based on VUU transport equations. Whereas for $K^+$ production in proton–nucleus reactions the secondary channel clearly dominates at subthreshold energies, $\eta$ mesons arise from primary and secondary processes with roughly the same order of magnitude. Detailed VUU calculations show that the relative weight of the various channels for nucleus–nucleus reactions is quite different as compared to the proton–nucleus case since $\Delta$-resonance excitation and inelastic $\Delta$–nucleon collisions are much more frequent.

## 1. Introduction

The production of heavy mesons at bombarding energies far below the free nucleon–nucleon threshold is of specific interest [1–5] as one hopes to learn either about cooperative nuclear phenomena or about high momentum components of the nuclear many-body wavefunction. While a lot of models have been proposed for $K^+$ production in proton–nucleus and nucleus–nucleus collisions [5–12], only few efforts have been invested for $\eta$-production [10, 13] where first experiments have recently been performed [14].

In this contribution we use a folding model for primary and secondary production processes based on Hartree–Fock initial groundstate momentum distributions [15, 16]. We briefly recapitulate the phase–space model in Section 2 and present results for $\pi^+$, $\eta$ and $K^+$ mesons for $p + {}^{12}C$ reactions up to 1.5 GeV. In Section 3 we compare the results of the folding model with those from semiclassical VUU simulations that are applied to $K^+$ and $\eta$ meson production in nucleus–nucleus collisions, too. A comparison with the first data from SIS shows that the observed meson yields can well be understood within the picture of incoherent hadron–hadron production channels.

## 2. Primary and secondary reaction channels

We briefly recall the assumptions of the folding model which is described in more detail in [15, 16]. The underlying picture is sketched in Fig. 1 for a $p + {}^{208}Pb$ collision at finite impact parameter $b$: A proton impinging on a nucleus at a bombarding energy $T_{lab} > 400\,\mathrm{MeV}$ is decelerated by the optical potential in the interior of the nucleus by about $U_{opt} \approx 40\,\mathrm{MeV}$ due to the momentum dependence of the effective in-medium nucleon–nucleon force [17, 18] before colliding with another nucleon. The first collision then happens at an average distance $\lambda_1 \approx (\sigma_{NN}\rho_0)^{-1} \approx 1.5\,\mathrm{fm}$ from the "nuclear surface". Apart from elastic scattering the proton may produce a heavy meson x with momentum $\boldsymbol{k}_x$ in the first collision. The Lorentz–invariant differential cross section to produce a meson in a proton–nucleon (pN) collision is then given by

$$\{E_x\, d^3\sigma_x^{NN}/d^3k_x\}_{prim.} = \int d^3p\, \{E'_x\, d^3\sigma_x^{e}(\sqrt{s})/d^3k'_x\}\rho(\boldsymbol{p}) \qquad (1)$$

where the Pauli-blocking factor for the final nucleon states has been neglected since kinematically the nucleons end up in an unoccupied regime in momentum space. In eq. (1) $\rho(\boldsymbol{p})$ stands for the target momentum distribution (normalized to 1) whereas the primed indices denote meson momenta in the individual nucleon–nucleon cms frame which have to be Lorentz-transformed to the detection frame, respectively. The quantity $\sqrt{s}$ is the invariant energy of the individual NN system.

The ansatz (1) physically implies that for primary production channels only the nuclear momentum distribution $\rho(\boldsymbol{p})$ is of relevance and thus involves an off-shell assumption with respect to stationary single-particle states. These off-shell phenomena have been investigated in detail in [19] for nucleus–nucleus collisions. There it was found that the quasiclassical energy–monentum relation holds already at quite low bombarding energy. This assumption, however, has not been proven so far for p + A reactions and remains a basic conjecture of the present approach.

The elementary differential cross section $d^3\sigma_x^e(\sqrt{s})/d^3k_x$ in eq. (1) is parameterized as a function of the maximum

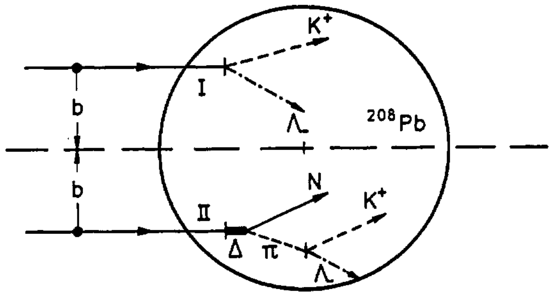


*Fig. 1.* Illustration of a $p + {}^{208}Pb$ collision at impact parameter $b$ for primary and secondary production of a $K^+\Lambda$ pair

* Supported by BMFT, GSI Darmstadt and Forschungszentrum Jülich.

† In collaboration with: A. Lang, U. Mosel, T. Vetter, K. Weber, Gy. Wolf, V. Metag (University of Giessen), O. W. B. Schult, W. Borgs, D. Gotta, A. Hamacher, H. R. Koch, H. Ohm, J. Pfeiffer, R. Riepe, H. Seyfahrt, K. Sistemich, V. Drüke, D. Filges, K. H. Watzlawik, R. Nellen, M. Karnadi, H. Stechemesser, G. Stollwerk (Forschungszentrum Jülich), B. Kamys, St. Kistryn, L. Jarczyk, P. Zolnierczuk, K. Pysz, J. Smyrski, A. Strzalkowski, B. Styczen (University of Cracow).

momentum $k_{\max}(\sqrt{s})$ as [5]

$$
\begin{aligned}
&E'_x \, \mathrm{d}^3\sigma_x^e(\sqrt{s})/\mathrm{d}^3k'_x \\
&\quad \approx \sigma_{\mathrm{pN}x}(\sqrt{s}) 3E'_x/(\pi k'^2_x k_{\max})(1 - k'_x/k_{\max})(k'_x/k_{\max})^2 \qquad (2)
\end{aligned}
$$

where $k_{\max}$ is given by

$$
\begin{aligned}
&k^2_{\max} = [s - (2m + m_\eta)^2][s - (2m - m_\eta)^2]/(4s) \quad \text{for } \eta\text{'s} \\
&k^2_{\max} = [s - (m + m_\Lambda + m_\mathrm{K})^2] \\
&\qquad \times [s - (m + m_\Lambda - m_\mathrm{K})^2]/(4s) \quad \text{for } \mathrm{K}^+ \qquad (3)
\end{aligned}
$$

with $\rho_{\mathrm{pN}x}(\sqrt{s})$ given by [5]

$$
\sigma_{\mathrm{pp}\eta}(\sqrt{s}) \approx \frac{0.17}{\mathrm{GeV}} \frac{\sqrt{s} - \sqrt{s_0}}{0.253\,\mathrm{GeV}^{-2} + (\sqrt{s} - \sqrt{s_0})^2} \quad [\mathrm{mb}],
$$

$$
\sigma_{\mathrm{pNK}^+}(\sqrt{s}) \approx 0.8 \left( \frac{k_{\max}}{\mathrm{GeV}/c} \right)^4 \quad [\mathrm{mb}]. \qquad (4)
$$

As indicated by the calculations in Ref. [20] we use $\sigma_{\mathrm{pn}\eta} \approx 3\sigma_{\mathrm{pp}\eta}$. In general one should note that the elementary cross sections $\sigma_{\mathrm{pN}x}(\sqrt{s})$ are not known properly especially close to threshold which introduces a quite sizeable uncertainty in the following calculations. The expressions for the differential pion cross sections $\sigma_\pi(\sqrt{s})$ are taken from an experimental data analysis of Ver West and Arndt [21].

Apart from the elementary differential cross section $\mathrm{d}^3\sigma_x^e/\mathrm{d}^3k$ the quantity (1) is determined by the momentum distribution $\rho(\boldsymbol{p})$ describing the available momentum components in a nucleus. We evaluate $\rho(\boldsymbol{p})$ in the mean-field limit, i.e. Hartree–Fock, thus neglecting the extreme momentum components due to residual two-body correlations.

Since the differential pion spectra as resulting from eq. (1) are presented in detail in [15], we only show that the first collision approach for pion production works rather well in the energy regime of interest. In this respect the differential cross section (1), multiplied by the number of first-chance collisions $N_1(A)$ as evaluated within the Glauber approximation ($N_1 \approx 7.3$ for $^{12}$C), is shown for $\pi^+$ production in Fig. 2 (upper dashed line) in comparison with the experimental data for $\mathrm{p} + {}^{12}\mathrm{C} \to \pi^+ + \mathrm{X}$ from [22–25] (full dots). The description of the data is quite accurate. We note that $\pi^+$ reabsorption has not been taken into account which is expected to be a minor effect for a light target such as $^{12}$C.

The results for $\eta$ and $\mathrm{K}^+$ production by first-chance pN collisions for $\mathrm{p} + {}^{12}\mathrm{C}$ are shown in Fig. 2 (middle and lower dashed lines, respectively) as a function of the proton laboratory energy $T_{\mathrm{lab}}$. Here, the first collision approximation clearly misses the experimental data for $\mathrm{K}^+$ production by Koptev *et al.* [12] by at least an order of magnitude and indicates that higher order processes [26–28] or even cluster production [29] may play an important role.

In order to evaluate the $\mathrm{K}^+$ production by the secondary processes $\pi\mathrm{N} \to \mathrm{K}^+\Lambda$ (cf. Fig. 1) we fold the primary pion distribution

$$
f_\pi(\boldsymbol{k}_\pi) = \{\mathrm{d}^3\sigma_\pi(\boldsymbol{k}_\pi)/\mathrm{d}^3k_\pi\}_{\mathrm{prim.}}/\sigma_{\mathrm{pN}} \qquad (5)
$$

with $\mathrm{d}^3\sigma_\pi/\mathrm{d}^3k_\pi$ from eq. (1) again with the nucleon momentum distribution $\rho(\boldsymbol{p})$ and the invariant production cross

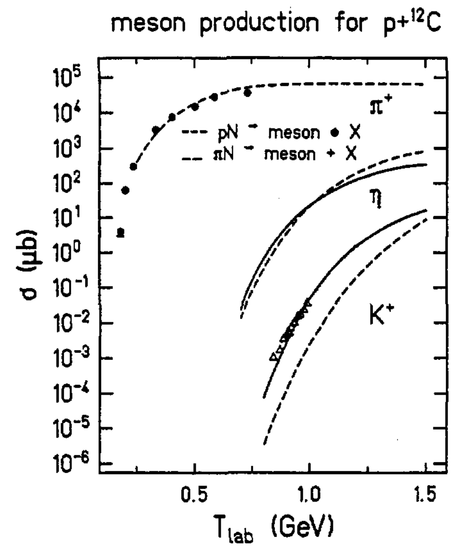


*Fig. 2.* Comparison of the calculated $\pi^+$ cross section (upper dashed line) as a function of the bombarding energy for $\mathrm{p} + {}^{12}\mathrm{C}$ with the experimental data from [22–25] (full dots). Also shown are the results for $\mathrm{K}^+$ production from pN (lower dashed line) and $\pi$N processes (lower solid line) in comparison to the data of Koptev *et al.* [12] (open triangles). The results for inclusive $\eta$ cross sections from pN and $\pi$N reactions are shown by the middle dashed and solid line, respectively, without accounting for $\eta$ reabsorption

section, i.e.

$$
\begin{aligned}
&\{E_\mathrm{K} \, \mathrm{d}^3\sigma_\mathrm{K}/\mathrm{d}^3k\}_{\mathrm{sec.}} \\
&\quad = \sum_\pi \iint \mathrm{d}^3p \, \mathrm{d}^3k_\pi \{E'_\mathrm{K} \, \mathrm{d}^3\sigma_{\pi\mathrm{N}\to\Lambda\mathrm{K}}(\boldsymbol{p}, \boldsymbol{k}_\pi)/\mathrm{d}^3k'\} \rho(\boldsymbol{p}) f_\pi(\boldsymbol{k}_\pi) \quad (6)
\end{aligned}
$$

where $\sum_\pi$ denotes the summation over the intermediate pion channels allowed by charge conservation. In case of $\mathrm{K}^+$ production this includes the channels $\pi^+\mathrm{n} \to \mathrm{K}^+\Lambda$ and $\pi^0\mathrm{p} \to \mathrm{K}^+\Lambda$. For $\eta$ mesons we only have to substitute the index K by $\eta$ in eq. (6) and to consider the channels $\pi^+\mathrm{n} \to \eta\mathrm{p}$, $\pi^0\mathrm{p} \to \eta\mathrm{p}$, $\pi^0\mathrm{n} \to \eta\mathrm{n}$ and $\pi^-\mathrm{p} \to \eta\mathrm{n}$. The (isospin averaged) differential cross section for secondary $\eta$ production is approximated by $\sigma_{\pi\mathrm{N}\to\eta\mathrm{N}} \approx 1/2\sigma_{\pi^-\mathrm{p}\to\eta\mathrm{n}}$ whereas the latter is parameterized by

$$
\sigma_{\pi^-\mathrm{p}\to\eta\mathrm{n}}(\sqrt{s}) \approx 13.07\,\mathrm{GeV}^{-0.5288}(\sqrt{s} - \sqrt{s_0})^{0.5288} \quad [\mathrm{mb}] \qquad (7\mathrm{a})
$$

for $\sqrt{s_0} = 1.486 < \sqrt{s} < 1.58906\,\mathrm{GeV}$,

$$
\sigma_{\pi^-\mathrm{p}\to\eta\mathrm{n}}(\sqrt{s}) \approx \frac{0.14486\,\mathrm{GeV}^{1.452426}}{(\sqrt{s} - \sqrt{s_0})^{1.452426}} \quad [\mathrm{mb}] \qquad (7\mathrm{b})
$$

for $\sqrt{s} \geqslant 1.58906\,\mathrm{GeV}$ which represents a fit to the well known experimental data for $\pi^-\mathrm{p} \to \eta\mathrm{n}$ [30] up to $\sqrt{s} = 4\,\mathrm{GeV}$. In case of $\mathrm{K}^+$ production the respective cross section is parameterized by [7]

$$
\sigma_{\pi^+\mathrm{n}\to\Lambda\mathrm{K}^+}(\sqrt{s}) \approx 9.89\,\mathrm{GeV}^{-1}(\sqrt{s} - \sqrt{s_0}) \quad [\mathrm{mb}] \qquad (8\mathrm{a})
$$

for $\sqrt{s_0} = m_\Lambda + m_{\mathrm{K}^+} \leqslant \sqrt{s} \leqslant 1.7\,\mathrm{GeV}$ and

$$
\sigma_{\pi^+\mathrm{n}\to\Lambda\mathrm{K}^+}(\sqrt{s}) \approx 0.09\,\mathrm{GeV}/(\sqrt{s} - 1.6\,\mathrm{GeV}) \quad [\mathrm{mb}] \qquad (8\mathrm{b})
$$

for $\sqrt{s} \geqslant 1.7\,\mathrm{GeV}$. The differential cross sections, furthermore, are assumed to be isotropic in the $\pi$N center-of-mass system and completely determined by energy and momentum conservation.

In order to calculate the production cross sections for p + A reactions we adopt the Glauber model which implies to multiply the folded cross sections (1) by the number of pN collisions. We recall that the number of first-chance nucleon–nucleon collisions $N_1(A)$ in this approximation gives $N_1(A) \approx A^{0.785}$ for $A \geqslant 15$ which is expected to hold with roughly 20% accuracy at the bombarding energy of interest. Furthermore, the number of events leading to meson production in secondary processes is approximated by $N_1(A)C(A)$, where the factor $C(A)$ accounts for the probability that a pion (produced in the first collision via the formation and decay of a $\Delta$ resonance) rescatters in the finite volume of the target. We assume the pion creation point for fixed impact parameter $b$ to be displaced from the nucler surface by $(\sigma_{pN}\rho_0)^{-1}$. Since the most energetic pions (that might produce an $\eta$ or $K^+$ meson in a $\pi$N collision) approximately move in beam direction, too, they propagate additionally by $(\sigma_{\pi N}\rho_0)^{-1}$ before a secondary collision takes place (cf. Fig. 1). This limits the impact parameter to $b^2 < R^2 - \lambda^2/4$, where $\lambda$ is given by

$$\lambda = \{\sigma_{pN}\rho_0\}^{-1} + \{\sigma_{\pi N}\rho_0\}^{-1} \approx 3.5\,\text{fm} \tag{9}$$

when inserting experimental values for the cross sections $\sigma_{pN}$ and $\sigma_{\pi N}$ at the energies of interest ($\rho_0 \approx 0.16\,\text{fm}^{-3}$). Integration over $b$ and normalization then yields the probability [15]

$$C(A) = (R^2 - \lambda^2/4)/R^2, \tag{10}$$

where $R \approx 1.2A^{1/3}$ [fm] is the radius of the target with mass number $A$.

The resulting cross sections for $\eta$ and $K^+$ production in p + $^{12}$C reactions are shown in Fig. 2 by the solid lines. We find that the $K^+$ data from Koptev *et al.* [12] are well reproduced when accounting for the secondary reaction channels. For $\eta$'s the primary and secondary reaction channels are approximately of the same order of magnitude. Please note that $\eta$-reabsorption is not taken into account in the global overview in Fig. 2. For further details on $\eta$ reabsorption we refer the reader to Ref. [16].

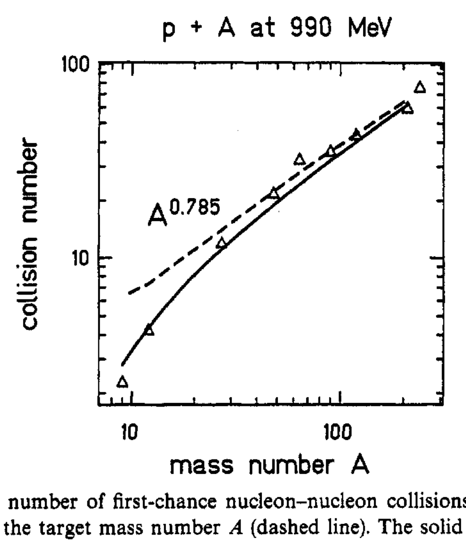


*Fig. 3.* The number of first-chance nucleon–nucleon collisions $N_1(A)$ as a function of the target mass number $A$ (dashed line). The solid line denotes the effective number of secondary processes according to eq. (10). The triangles represent the experimental data [12] at 990 MeV each divided by 9.1 nb

The conjecture that at energies below 1 GeV the kaons are primarily produced by the $\pi$N channels is supported by the mass dependence at $T_{lab}$ = 990 MeV, which is shown in Fig. 3 by the triangles where we have divided the experimental data [12] by $\sigma$ = 9.1 nb which is the calculated $K^+$ cross section per pion–nucleon collision at this energy. The first-chance collision number $N_1(A)$ (dashed line) sincerely misses the $A$-dependence for low masses whereas the number of secondary collision events $N_2(A) \approx N_1(A)C(A)$ (solid line) quite nicely reproduces the experimental trend.

## 3. Comparison to VUU simulations

The simplicity of the folding model (Section 2) allows for a rather fast evaluation of differential meson cross sections in p + A reactions and thus provides a more global view on systematics with respect to mass $A$ and projectile energy $T_{lab}$ provided that it is also supported by more microscopic calculations, e.g. of the VUU type [5, 31]. Since a detailed description of particle production in the framework of transport approaches has been given in a recent review [5] we do not present any further equations and discussion of numerical implementations. The only quantities of interest are the parameterization of the elementary process pN $\rightarrow$ N$\Lambda$K$^+$, $\pi$N $\rightarrow$ $\Lambda$K$^+$, which we take to be the same for the comparison, and the initial condition for the target momentum distribution $\rho_{VUU}(p)$ in the VUU simulation. As described in [5] the distribution $\rho_{VUU}(p)$ – that is adopted in the initialization – is very close to Hartree–Fock results for momenta $p \leqslant p_F$ (Fermi momentum), however, lacks high momentum components $p > p_F$ in line with the semiclassical approximations performed in the derivation of the transport theory. We thus expect differences to appear especially for low bombarding energies.

### 3.1. *Proton–nucleus collisions*

Since at very low subthreshold energies the cross sections of the relevant elementary processes are very small, we propagate N's and $\Delta$'s but treat pions perturbatively, i.e. a pion is produced in given nucleon–nucleon collision with a differential probability according to the Ver West and Arndt prescription [21] in the same way as in the folding model (Section 2). The only difference thus is a discrete (space–time localized) description of NN collisions in the VUU approach. The second step reactions $\pi$N $\rightarrow$ $\Lambda$K$^+$ are treated by folding the individual pion probability $f_i(\boldsymbol{k}_\pi)$ from each individual NN collision $i$ over all discrete nucleon momenta $\boldsymbol{k}_N$ in a volume of 33 fm$^3$ around the creation point $r_i$ of the pion. The volume of 33 fm$^3$ corresponds to a sphere of radius 2 fm which reflects the pions average mean-free-path $\lambda_\pi = (\sigma_{\pi N}\rho_0)^{-1} \approx 2$ fm. We, furthermore, have neglected the fact that the pion is produced by the decay of a baryonic resonance which propagates in the nuclear medium by about 0.5–1 fm and accidentally might decay outside the nucleus in case of very light nuclei. For the purposes of the present investigation we only note that the final $K^+$ cross section from $\pi$N reactions changes by at most 20% when changing the radius parameter by a factor of 2 for $A \geqslant 12$. The numerical results for p + $^{12}$C [32] as shown in Fig. 4 in comparison to the data of Koptev *et al.* [12] and demonstrate the dominance of the $\pi$N channels for $K^+$ production

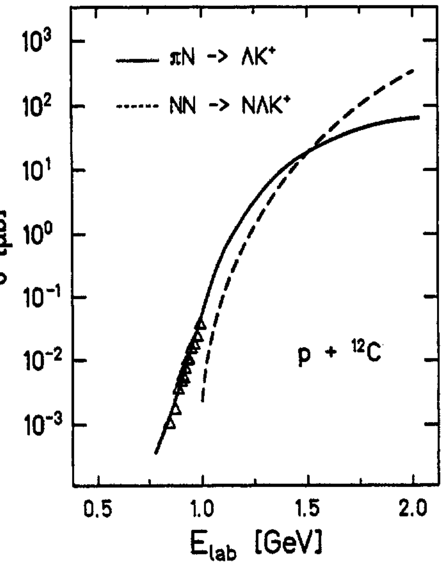


*Fig. 4.* Results of VUU calculations for $K^+$ production in p + $^{12}$C reactions for primary (dashed line) and secondary channels (solid line) in comparison to the data [12]

in the same way as the folding model. Note that due to the lack of higher momentum components there are no kaons from the primary channel below 1 GeV. This restriction, however, does not seriously change the result for the secondary channel since here the Fermi motion is exploited twice.

### 3.2. $K^+$ *Production in nucleus–nucleus collisions*

Since the VUU approach has been especially developed for heavy-ion reactions at intermediate and high bombarding energy [5, 31], we can use the same approach for A + A collisions and study the contribution of the various channels as a function of bombarding energy. The numerical results for $^{40}$Ca + $^{40}$Ca from 0.6 to 1.6 GeV/u are shown in Fig. 5 where the dashed line reflects the $K^+$ yield from $\pi$N reactions which is small at all bombarding energies compared to the baryon–baryon production channels (solid line) [33, 34]. As will be discussed below, the dominant production channels are those involving an intermediate resonance [$\Delta$(1232)]. Thus there are no simple extrapolations from $K^+$ cross sections in p + A reactions to nucleus–nucleus collisions.

As suggested by Aichelin and Ko some years ago [11], $K^+$ cross sections might be used to determine the compressibility of nuclear matter. We investigate the latter problem within a fully covariant transport approach (RBUU) – that properly accounts for momentum-dependent forces [35] – by adopting the Lorentz invariant differential cross section in the parametrization by Zwermann [9] for the channels $BB \to K^+\Lambda B$ or $\to K^+\Sigma B$. For the detailed evaluation of the differential $K^+$ spectra we refer the reader to the paper by Lang *et al.* [36] and only present the final results.

In Fig. 6 we show the inclusive differential $K^+$ and single proton spectra at $\theta_{lab} = 41°$ for Au + Au and Ne + Ne at 1 GeV/u employing the parametersets NL1 (solid lines), NL2 (dashed lines) and NL3 (dotted lines). The parametersets NL1 and NL2 exhibit the same strength of the momentum dependent forces (i.e. $m^*/m = 0.83$) but differ in the compressibility ($K = 380$ MeV for NL1; $K = 210$ MeV for NL2) while NL3 leads to the same compressibility as NL1 but differs in the effective mass ($m^*/m = 0.7$ at $\rho_0$) and thus leads to stronger Lorentz forces. Whereas for the light system Ne + Ne essentially no dependence on the compressibility $K$ is found we observe a factor of about 3 for Au + Au when comparing the results for the "stiff" EOS (NL1; solid line) with those of the "soft" EOS (NL2; dashed line).

Since experimentally the ratio of $K^+$ mesons to single protons can be determined more easily in the spectrometer,

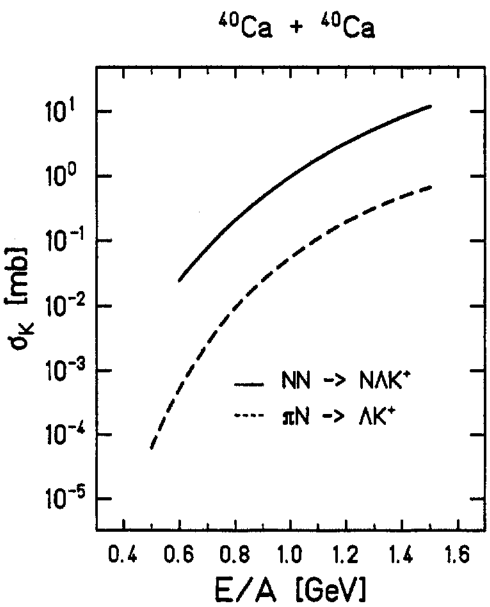


*Fig. 5.* Calculated $K^+$ cross section for $^{40}$Ca + $^{40}$Ca as a function of bombarding energy for baryon (solid line) and pion (dashed line) induced production channels

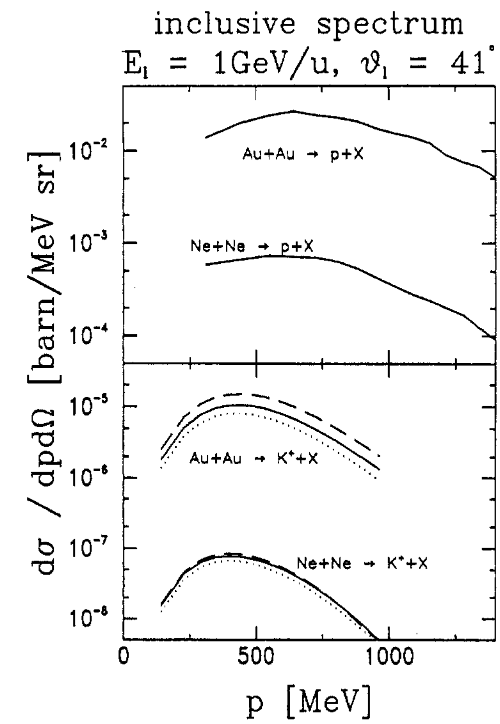


*Fig. 6.* Differential $K^+$ and single proton spectra for Au + Au and Ne + Ne at 1 GeV/u for the parametersets NL1 (solid lines), NL2 (dashed lines) and NL3 (dotted lines) (see text)

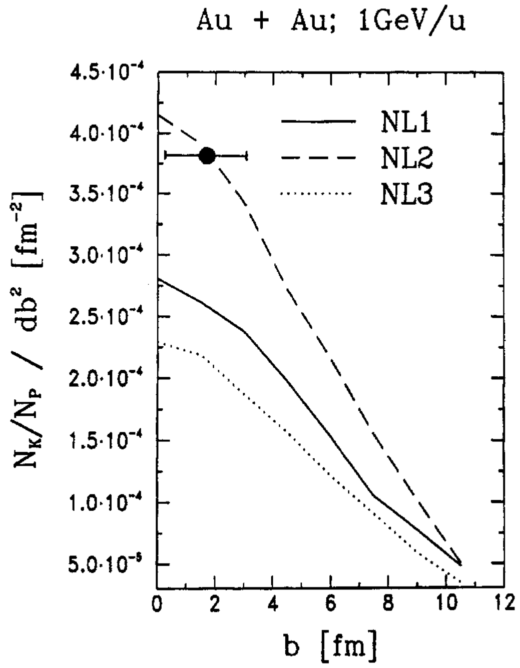


*Fig. 7.* Ratio of the total $K^+$ to single proton yield as a function of the impact parameter $b$ for $\theta = 41°$. Solid line: NL1; dashed line: NL2; dotted line: NL3. The data point is taken from Ref. [37]

we show in Fig. 7 the respective ratio as a function of the impact parameter $b$ for the three parametersets in comparison to the experimental ratio of $3.8 \times 10^{-4}$ from Ahner *et al.* [37] for central collisions of Au + Au. This comparison clearly favors the "soft" EOS described by the parameterset NL2. However, one has to keep in mind that most of the $K^+$ mesons at this energy are produced by the channel $N + \Delta \rightarrow K^+ + X$ (Fig. 8) where the elementary cross section is barely known. In this respect one has to look preferentially at $K^+$ ratios from light and heavy systems since then ambiguities in the elementary cross section cancel out to a large extent [36].

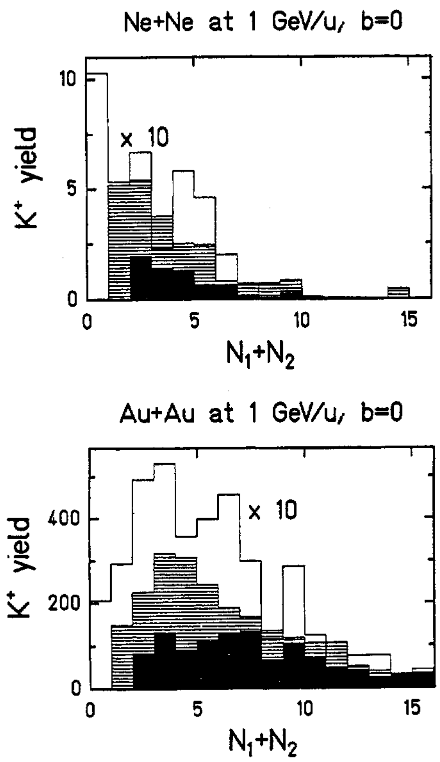


*Fig. 8.* Baryonic decomposition of the collisions producing a $K^+$ for Ne + Ne and Au + Au at 1 GeV/u and $b = 0$. Open histograms: nucleon–nucleon collisions ($\times 10$); hatched histogram: nucleon–$\Delta$ channel; filled histogram: $\Delta$–$\Delta$ channel

### 3.3. $\eta$ *Meson production in nucleus–nucleus collisions*

Whereas $K^+$ mesons couple only weakly to the baryonic environment and thus their production can be treated perturbatively, this does no longer hold for $\eta$ mesons due to their strong final interactions. In order to keep track of the various interaction channels we have developed a transport approach where nucleons and nucleon resonances [$\Delta(1232)$, N(1440), N(1535)] are propagated explicitly with their isospin degrees of freedom as well as pions and $\eta$'s [38, 39]. Here the nucleon resonances move within the same time-dependent mean field as the nucleons whereas pions and $\eta$'s are treated as free particles. Pion production is assumed to be entirely due to the formation and decay of the resonances with experimental branching ratios while $\eta$ production proceeds through the excitation of an N(1535) resonance which decays by roughly 50% to the N + $\eta$ channel. The individual formation cross sections are adopted from [21] or [16], respectively, whereas time reversed channels are evaluated by detailed balance [39].

Within this nonperturbative approach we find – as expected – that above threshold ($>1.256$ GeV) most $\eta$'s are produced in nucleon–nucleon (N + N) collisions. This is shown in Fig. 9 which displays the various production channels for primordial $\eta$'s as a function of bombarding energy for central collisions of $^{40}Ca + ^{40}Ca$. However, below threshold nucleon–resonance (N + R) production channels become important, too. It is worth noting that the $\pi$ + N channel supersedes the N + R processes above about 1 GeV but is less important below. The large enhancement of N + R channels in nucleus–nucleus collisions as compared to p + A reactions is due to the fact that $\eta$ meson production in A + A reactions takes place at rather high densities ($2$–$3\rho_0$) [38] such that on average the $\Delta$ resonance rescatters with the nucleon instead of decaying to $\pi$ + N as in case of p + A reactions.

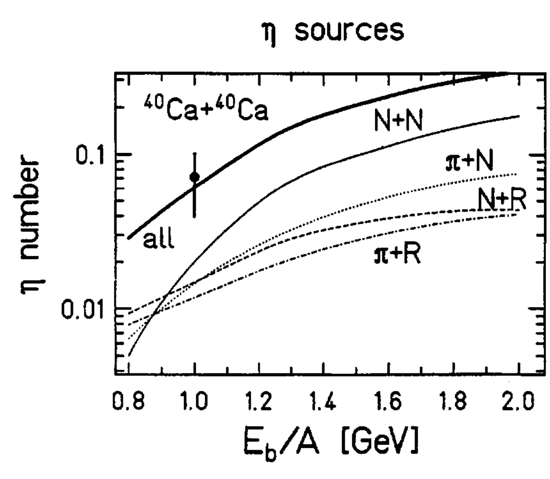


*Fig. 9.* Hadronic decomposition of the $\eta$ meson production channels for $^{40}Ca + ^{40}Ca$ collisions as a function of the bombarding energy per nucleon from Ref. [39]. The experimental data point at 1 GeV/u is taken from [40]

A detailed analysis of the $\eta$ rescattering and reabsorption processes, furthermore, indicates that the asymptotically observed $\eta$'s no longer carry essential information from the high density phase of the reaction since their last interaction vertex takes place at rather low density [38]. When comparing our calculations – scaled in Fig. 9 to the asymptotic number of $\eta$'s emerging from the simulation – to the experimental data point from Metag *et al.* [40], we find no serious discrepancy which implies that the dominant reaction channels are met in our transport approach.

## 4. Summary

In this contribution we have presented calculations for $K^+$ and $\eta$ production in p–nucleus reactions based on on-shell scattering processes and uncorrelated Hartree–Fock momentum distributions. This approach quite accurately reproduces pion as well as $K^+$ yields in proton induced reactions and compares well with VUU calculations for these reactions. Whereas in case of $\eta$ production primary and secondary channels are roughly of the same order of magnitude, the production of $K^+$ mesons is found to be dominated by the secondary channel $\pi N \to K^+\Lambda$ up to 1.5 GeV. The latter result is essentially due to the fact that via secondary reactions one can exploit the internal Fermi motion twice and thus shift the production threshold substantially to lower energies. Furthermore, the cross section $\sigma_{\pi N \to \Lambda K^+}$ is large compared to $\sigma_{pn \to n\Lambda K^+}$ above threshold.

The secondary reaction mechanism is furthermore supported by the experimental mass dependence of the $K^+$ inclusive cross sections. This becomes striking especially for light targets such as $^9$Be or $^{12}$C. On the other hand, one cannot simply extrapolate $K^+$ cross sections from $p + A$ reactions to nucleus–nucleus collisions since the reaction channels are quite different. Detailed VUU calculations even show that in lowest order the pion induced production channels for $K^+$ mesons in $A + A$ collisions can be neglected.

We have also discussed that the subthreshold production of $K^+$ mesons in Au + Au collisions yields information on the compressibility of cold nuclear matter since their yield and spectra increase by up to a factor of 3 when decreasing the compressibility from $K = 380\,\text{MeV}$ to $K = 210\,\text{MeV}$. However, due to unknown production cross sections especially for the dominant channel $N + \Delta \to K^+ + X$ the absolute spectra are rather uncertain and one has to examine production ratios for light and heavy systems to determine the compressibility $K$ in an approximately model-independent way.

The production of $\eta$'s in nucleus–nucleus collisions was calculated nonperturbatively via the formation and decay of the N(1535) resonance including $\eta$ rescattering and reabsorption. Though the existing experimental data point from Metag [40] is met quite well, it is too early to draw any final conclusions on $\eta$ dynamics at high nuclear densities since the various final state interactions strongly distort the information from the high density phase.

## References

1. Grimm, P. and Grosse, E., Prog. Part. Nucl. Phys. **15**, 339 (1985).
2. Braun-Munzinger, P. and Stachel, J., An. Rev. Nucl. Part. Sci. **37**, 1 (1987).
3. Jakobsson, B., this volume.
4. Shyam, R. and Knoll, J., Nucl. Phys. **A426**, 606 (1984); **A483**, 711 (1988).
5. Cassing, W., Metag, V., Mosel, U. and Niita, K., Phys. Rep. **188**, 363 (1990).
6. Randrup, J. and Ko, C. M., Nucl. Phys. **A343**, 519 (1980); **A411**, 537 (1983).
7. Cugnon, J. and Lombard, R. M., Nucl. Phys. **A422**, 635 (1984).
8. Zwermann, W. and Schürmann, B., Nucl. Phys. **A423**, 525 (1984).
9. Zwermann, W., Mod. Phys. Lett. **A3**, 251 (1988).
10. Schürmann, B. and Zwermann, W., Mod. Phys. Lett. **A3**, 1441 (1988).
11. Aichelin, J. and Ko, C. M., Phys. Rev. Lett. **55**, 2661 (1985).
12. Koptev, V. P., Mikirtych'yants, S. M., Nesterov, M. M., Tarasov, N. A., Shcherbakov, G. V. *et al.*, Sov. Phys. JETP **67**, 2177 (1988).
13. De Paoli, A. L., Niita, K., Cassing, W. Mosel, U. and Ko, C. M., Phys. Lett. **219B**, 194 (1989).
14. Chiavassa, E., Della Casa, G., De Marco, N., Ferrero, F., Musso, A. *et al.*, Nucl. Phys. **A519**, 413c (1992); Berg, F. D., Boonstra, A., Braak, H. P., Brummund, N., Döring, W. *et al.*, Z. Phys. **A340**, 297 (1991).
15. Cassing, W., Batko, G., Mosel, U., Niita, K., Schult, O. and Wolf, Gy., Phys. Lett. **238B**, 25 (1990).
16. Cassing, W., Batko, G., Vetter, T. and Wolf, Gy., Z. Phys. **A340**, 51 (1991).
17. Hama, S., Clark, B. C., Cooper, E. D., Sherif, H. S. and Mercer, R. L., Phys. Rev. **C41**, 2737 (1990).
18. Weber, K., Blättel, B., Cassing, W., Dönges, H. C., Koch, V., Lang, A. and Mosel, U., Nucl. Phys. **A539**, 713 (1992).
19. Cassing, W., Z. Phys. **A326**, 21 (1987); Z. Phys. **A327**, 87 (1987).
20. Vetter, T., Biro, T. S., Engel, A. and Mosel, U., Phys. Lett. **263B**, 153 (1991).
21. Ver West, B. J. and Arndt, R. A., Phys. Rev. **C25**, 1979 (1982).
22. Bimbot, L., Bellini, V., Bolore, M., Charlot, X., Guet, C. *et al.*, Nucl. Phys. **A440**, 636 (1985).
23. DiGiacomo, N. J., Clover, M. R., De Vries, R. M., Dousse, J. C., Kapustinsky, J. S. *et al.*, Phys. Rev. **C31**, 292 (1985).
24. Crawford, J. F., Daum, M., Eaton, G. H., Frosch, R., Hirschmann, H. *et al.*, Phys. Rev. **C22**, 1184 (1980).
25. Krasnov, V. A., Kurepin, A. B., Reshetin, A. I., Oganesjan, K. O. and Pasyuk, E. A., Phys. Lett. **108B**, 11 (1982).
26. Komarov, V. I. *et al.*, Nucl. Phys. **A326**, 397 (1979).
27. Nesterov, M. M. and Tarasov, N. A., Sov. Phys. JETP **59**, 226 (1984).
28. Tarasov, N. A., Koptev, V. P. and Nesterov, M. M., Pis'ma Zh. Eksp. Teor Fiz. **43**, 217 (1986).
29. Müller, H., Z. Phys. **A339**, 409 (1991).
30. in: "Landolt–Börnstein" (Edited by O. Madelung) (Springer, Berlin–Heidelberg–New York 1988), vol. NS I/12.
31. Bertsch, G. F. and Das Gupta, S., Phys. Rep. **160**, 189 (1988).
32. Cassing, W., Batko, G., Blättel, B., Koch, V., Lang, A. *et al.*, Nucl. Phys. **A519**, 357c (1990).
33. Batko, G., Cassing, W., Mosel, U., Niita, K. and Wolf, Gy., in: "Proceedings of the International Workshop on Gross Properties of Nuclei and Nuclear Excitations, XVIII, Hirschegg, Austria, 1990" (Edited by H. Feldmeier) (Darmstadt 1990), p. 174.
34. Xiong, L., Ko, C. M. and Wu, J. Q., Phys. Rev. **C42**, 2231 (1990).
35. Cassing, W. and Mosel, U., Prog. Part. Nucl. Phys. **25**, 235 (1990).
36. Lang, A., Cassing, W., Mosel, U. and Weber, K., Nucl. Phys. **A541**, 507 (1992).
37. Ahner, W., Baltes, P., Bormann, Ch., Brill, D., Brockmann, R. *et al.*, Z. Phys. **A341**, 123 (1991).
38. Wolf, Gy, Cassing, W. and Mosel, U., Phys. Lett. **B271**, 43 (1991).
39. Wolf, Gy., Cassing, W. and Mosel, U., Nucl. Phys. **A545**, 139c (1992).
40. Metag, V., in: "Proceedings of the VI International Conference on Nuclear Reaction Mechanisms, Varenna, June 1991" (Edited by E. Gadioli) (Milano 1991), p. 683.